TÜBİTAK

Turkish Journal of Chemistry

http://journals.tubitak.gov.tr/chem/

Research Article

Turk J Chem
(2021) 45: 661-672
© TÜBİTAK
doi:10.3906/kim-2012-19

Evaluation of the fuel cell performances of TiO_2/PAN electrospun carbon-based electrodes

Sema ASLAN*
Departmentof Chemistry, Faculty of Science, Muğla Sıtkı Koçman University, Muğla, Turkey

Received: 09.12.2020 • **Accepted/Published Online:** 12.02.2021 • **Final Version:** 30.06.2021

Abstract: Electrocatalytic effect of the untreated and TiO_2+polyacrylonitrile (PAN) modified discarded battery coal (DBC) and pencil graphite electrodes (PGE) were evaluated in fuel cell (FC) applications. TiO_2+PAN solution is coated on PGE and DBC electrodes by electrospinning. According to the FESEM and EDS characterizations, TiO_2 and PAN nanofibers are found to be approximately 40 and 240 nm in size. TiO_2+PAN/PGE showed the best FC performances with 2.00 A cm^{-2} current density and 5.05 W cm^{-2} power density values, whereas TiO_2+PAN/DBC showed 0.68 A cm^{-2} current density and 0.62 W cm^{-2} power density values. Electrochemical characterizations of PGE and TiO_2+PAN/PGE electrodes were investigated by cyclic voltammetry and electrochemical impedance spectroscopy. Finally, long-term FC measurement results of developed electrodes exhibited very reasonable recovery values. Along with the comparison of the electrode performances, the recovery of DBCs as electrodes for renewable energy production has been achieved.

Key words: Battery, fuel cell, pencil graphite electrode, hydrogen production, electrospinning, recovery

1. Introduction

Nanoparticle modified nanofibers have been successfully applied in divergent areas such as catalysis [1–3], tissue engineering [4], photochemical applications [5–7], capacitors [8], energy applications [9], membrane electrodes in fuel cells[10], etc... Fuel cells (FC) are environmentally friendly alternative power sources [11] and until now, from solid oxide to microbial FCs, various studies have been reported, which use the advantage of electrospun polymers [10,12–15]. Electrospun polymers exhibit unique electrochemical activity. Besides, nanomaterial supported 1D nanofibers can be used as a useful tool due to their small diameters and highly porous structures. Therefore, they gained attention by the electrochemical researchers for the electrode surface modification studies [16].

Polyacrylonitrile (PAN) is the most widely used carbon nanofiber precursor due to its high carbon content [17], besides, it is thermally stable and it provides a highly directable molecular structure [18,19]. Zhang et al. (2020) [20] reported that higher PAN content caused higher permeability and conductivity on FC performance. Padmavathi et al. (2013) [18] used Pt-loaded PAN carbon nanofiber in the FC proton exchange membrane. Also, PAN has a very suitable environment for immobilizing nanomaterials. Its carbon-rich nature can be improved by the addition of electrochemical redox-triggering nanomaterials [21]. There have been reported many nanomaterials modified PAN utilized applications, especially on Li-ion batteries [22] or dye-synthesized solar cells [23]. Although, Pt nanoparticle including PAN nanofibers are very effective catalysts in FC applications [24], here we have suggested an alternative cost-effective and useful way. The catalytic effect on the recovered carbon electrode surface is achieved by the combination of PAN and TiO_2 nanostructures instead of expensive noble- or semi-noble metal nanoparticles [21–26].

TiO_2 nanostructures are generally preferred towards electrode modifications because of their film-forming capabilities, high surface area, optical transparency, biocompatibility, and good conductivity [27]. Beginning with the first report on the excellent shuttle effect of TiO_2 nanoparticles on solar cells in dye-synthesized solar cells by O'Regan and Gratzel (1991) [28], researchers quickly improved their work in the optical field. Its superiority in photocatalytic studies has overshadowed its use for other power applications [29]. However, thanks to its mesoporous structure, there is a respectable number of TiO_2 nanoparticle using FC applications [30–32]. Generally, PAN and TiO_2 nanostructures are used as carbide derivatives in electrocatalytic applications. [33]. In addition, a comparative study on the catalytic activity and stability of TiO_2, TiN, and TiC-supported Pt electrocatalysts for the oxygen reduction reaction in the proton exchange membrane

* Correspondence: semaaslan@mu.edu.tr

fuel cells has been reported by Mirshekari and Shirvanian (2019) [34]. Also, Tański et al. (2017) reported a study on the analysis of the optical properties and the energy band structure of PAN/TiO_2 nanoparticles in the form of thin composite nanofibrous mats [35]. Similarly, some new materials, such as carbon nanotube/polyaniline composite [36], titanium dioxide/polyaniline composite [37,38], have been used as anodes in MFCs and exhibited high current densities [39].

The use of pencil graphite electrodes (PGE) is very common in electrochemical applications [40,41] among other graphite-based electrodes because of its ease of use and purchase, cost-effectiveness, and wearable electrodes. However, waste recovery for catalytic or energy applications is another developing area [42,43]. Especially, waste battery materials are used for their metal components [44], such as lead [45] or cobalt [46]. Chemical or electrochemical methods are used for the recovery process. Discarded battery coals (DBCs) are often used for previous electrical tests of electrical work with good conductivity and large surface area. Therefore, its components and conductivity still need to be investigated after the battery conditions are used. However, our group has recently published a study on the examination of the TiO_2+PAN coated discarded battery coal (DBC) electrode as a supercapacitor [47] and also Zr and Ce modified DBC electrodes successfully applied in electrolysis cells [48]. In the supercapacitor application, mostly capacitive properties of the developed electrode were investigated and evaluated as a good candidate for FC applications.

The electrospinning of DBCs was first investigated in FC applications in the scope of the presented study. The obtained results were found to be significantly improved. Although the pencil graphite electrode (PGE) shows the best FC performances in the presented study, the usage of the DBC is the main innovation of this research and is worth developing. DBC and PGE are specified as carbon-based electrodes. TiO_2 nanoparticles were suspended in PAN, and electrospinning was performed on the DBC and PGE electrodes (Figure 1).

The characterization of the morphological features of nanoparticles and nanofibers was performed by field emission scanning electron microscopy (FESEM) with energy-dispersive X-ray spectroscopy (EDS), and X-ray diffraction (XRD) measurements. Untreated and TiO_2+PAN modified DBC and PGE electrodes were used as cathodes to evaluate the electrocatalytic effect of nanoparticle modified nanofibers in FC applications. In addition, the electrochemical characterization of the PGE and TiO_2+PAN/PGE electrodes was investigated by cyclic voltammetry (CV) and electrochemical impedance spectroscopy (EIS) measurements. Finally, the long-term FC measurement results of the developed electrodes showed reasonable recovery values and found to be promising and practically feasible.

2. Experimental

2.1. Materials

Titanium (IV) n-butoxide ($Ti(OBu)_4$) in isopropyl alcohol (ipa), acetylacetone, nitric acid (HNO_3) (analytical grade, 99.9%), sodium nitrate ($NaNO_{3(aq)}$), sodium hydroxide (NaOH) (analytical grade, 98% pure), polyacrylonitrile (PAN)

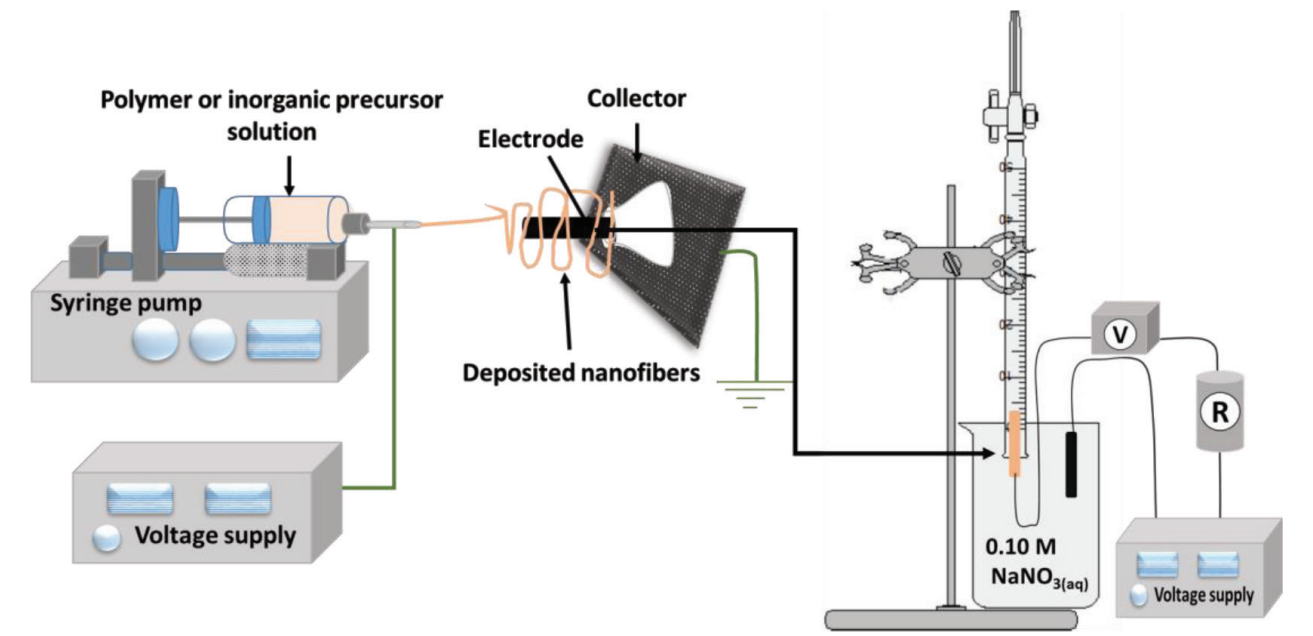

Figure 1. Schematic diagram of the electrospinning setup and FC design.

(Mw ~ 150,000), and N,N-dimethylformamide (DMF) (99.8%) were purchased from Sigma-Aldrich (Sigma-Aldrich Corp., St. Louis, MO, USA). PGE (Tombow, 0.9 mm) was purchased from a local stationary, DBCs were used from the recovery bins of university (used up Panasonic AA R6 Zinc Carbon 1.5V batteries were used).

2.2. Electrospinning system

Figure 1 shows a schematic diagram of the electrospinning of TiO_2+PAN set up and the apparatus used in this study which consist of a high-voltage power supply, a syringe used as polymer precursor solution reservoir, a syringe pump, collecting plate (covered with aluminum foil), a cone adapter was used for the fixation of electrodes in the upright position to the collector plate. The electrospinning setup is purchased from Inovenso Ltd. Firstly, 10% (w v^{-1}) TiO_2 nanoparticles were suspended in the 10% PAN including DMF solution for 24 h in a sonicator. A positive voltage of 20 kV was applied to the stainless steel needle therewithal to the TiO_2+PAN polymer solution during the electrospinning process. For grounding, the electrode was connected to DBC or PGE electrodes located on a metallic plate in the upright position (Figure 1) with 15 cm distance. Electrospun fibers were collected at the rate of 0.5 mL s^{-1} on the electrodes by rotating the electrodes manually [2].

2.3. Preparation of TiO_2 nanoparticles

The TiO_2 was prepared according to a modified sol–gel method [27] Titanium (IV) *n*-butoxide ($Ti(OBu)_4$) in isopropyl alcohol (ipa) solution was used as the precursor of TiO_2. Acetylacetone (acac) was used to moderate the reaction rate. The molar ratio of the reactants was: $Ti(OBu)_4$:H_2O:ipa:acac = 1:100:2:0.01. Firstly, deionized water was carefully dropwise added to ($Ti(OBu)_4$) containing ipa solution for hydrolysis according to the given ratios above. The resulting white precipitate of titanium oxyhydroxide was rinsed by water a couple of times. The final solution was treated with HNO_3, then refluxed at 85 °C for 8 h up to give a sol (pH ~2.5). Then the sol processed to drying at 100 °C for 3 h in a drying oven, then calcinated in the furnace at 500 °C to give TiO_2 nanopowder.

2.4. Fuel cell studies

The structure of the FCs was shown in Figure 1. The FC was composed of a 400 mL single-cell compartment, anode, and cathodes. Geometrical surface areas of the cathodes were about 0.22 cm^2 and 0.06 cm^2 for DBC and PGE based electrodes (the geometrical surface areas were calculated according to $2\pi rh+\pi r^2$). A multimeter and power supply were utilized for the current-potential readings. A series of resistances ranging from 1 Ω to 10 M Ω were used to obtain polarization graphs. 0.1 M 200 mL of $NaNO_{3(aq)}$ solution was filled into the cell and served as the electrolyte. Measurements were recorded at room temperature and atmospheric pressure. Both the anode and cathode electrodes were immersed into the electrolyte. Electrical connections were provided with crocodiles. Firstly, power (P=IxV) and current (I=V/R) values are calculated then power and current density values are calculated by dividing obtained current values into the geometrical surface area of the cathode electrodes. Obtained power and current densities were plotted vs. potential values obtained from the FC system. Polarization graphics show the maximum power and current density values and the best potential value of the FC systems. FC systems were measured at 3.5 V and 9 V external potentials. All of the experiments were replicated for three times.

2.5. Electrochemical measurements

As a result of FC measurements, the best power and current output values were obtained from PGE and TiO_2+PAN/PGE electrodes. Thus, these electrodes were investigated in terms of the electrochemical activity by CV and EIS methods. Autolab PGSTAT 204 potentiostat/galvanostat (Metrohm Autolab B.V.) electrochemical station equipped with FRA module and driven by NOVA 2.1.4 software was used. PGE or TiO_2+PAN/PGE were utilized as working electrodes in a three-electrode cell where Ag/AgCl (containing 3 M KCl, CHI115) was the reference and Pt (CH Instruments Inc. CHI 111) served as the counter electrodes in 6 M KOH electrolyte. CV measurements were recorded at the potential range of −0.3 to 0.6 V at the scan rate of 100 mV s^{-1}. EIS was measured in a frequency range of 10^{-1} to 10^{-4} Hz in 6 M KOH solution.

3. Results and Discussion

3.1. Preparation and characterization of TiO_2 nanoparticles and TiO_2/PAN composite fibers

It has been pointed at the literature that [27] the pH value control is crucial on the obtaining final size of TiO_2 particles during the process. Titanium (IV) n-butoxide is appointed as an effective precursor for TiO_2 synthesis since a stable sol can be obtained at the harshly acidic condition at pH < 2. Besides, the heat treatment after preparation is another important parameter and can be adjusted according to the desired final composition and microstructure. Firstly, anatase nucleates occurre as the initial kinetic product. Subsequently, the higher calcination temperature leads to phase transformation from anatase to a more stable rutile phase. The fraction of the rutile phase increases by calcination temperatures [49]. The XRD measurements of TiO_2 nanoparticles showed typical TiO_2 peaks related to the anatase, and rutile phases (Figure 2). XRD

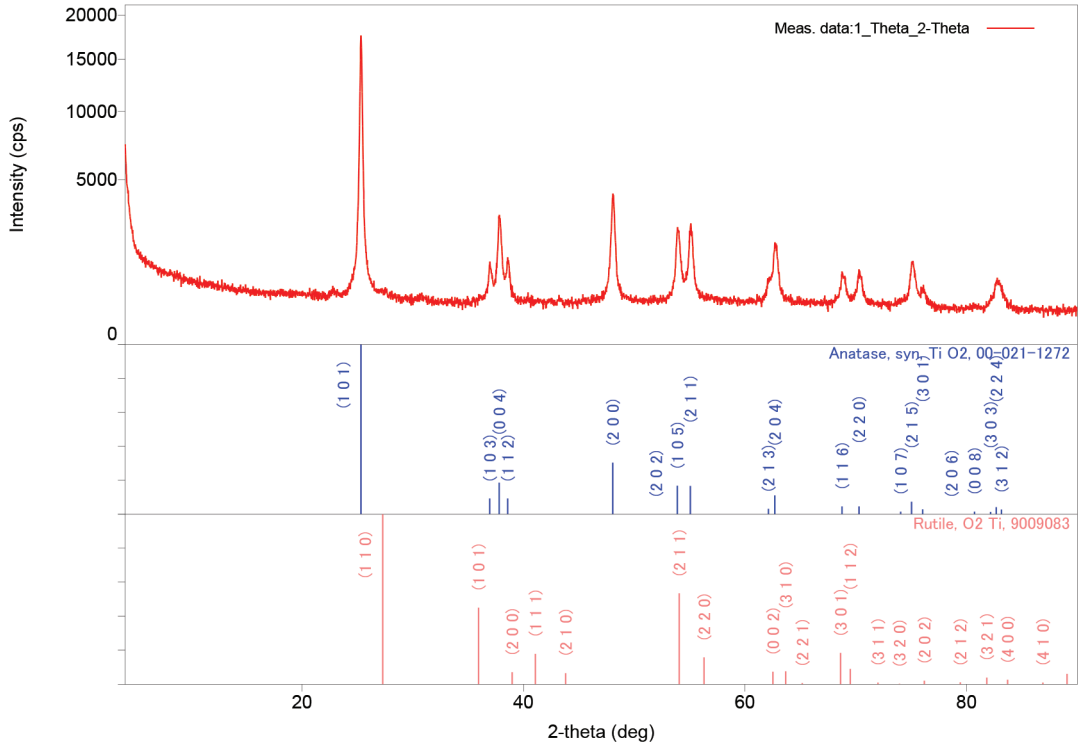

Figure 2. XRD measurements of TiO_2 nanoparticles for both anatase and rutile phases.

patterns exhibited strong diffraction peaks at 25° and 48° indicating TiO_2 in the anatase phase. On the other hand, the peaks observed at 26°, 37° and 55° indicating TiO_2 in the rutile phase. All peaks are in good agreement with the standard spectrum (JCPDS no.: 88-1175 and 84-1286). The results from XRD indicate that the main phase is anatase but the rutile phase is also observed. Obtained results are in accordance with the given literature [49] at 500 °C measurements.

FESEM and EDS results of the synthesized TiO_2 nanoparticles (Figure 3C, 3B, and 3E) are measured as approximately 40 nm-sized. Atomic and weight percentages are given as inset for both of the PAN+TiO_2 and TiO_2 nanostructures. Presence of Al and Au elements in the EDX spectrum of PAN+TiO_2 are because of the aluminum foil that is used as s collector during electospinning, and, for the imaging of polymeric PAN nanofibers by FESEM, Au coating is needed. The ratios of TiO_2 nanoparticles are very reliable and consistent for nanofiber encapsulated and natural states. Here, the ratios of the reactants were maintained as reported in the literature, but the calcination temperature was taken as average (500 °C).

Fundamentally the electrospinning is an advanced process that utilizes high DC voltage between a capillary and a conductive surface for the production of delicate nanofibers. In the process a specific electric field is applied to the system when this voltage overcomes the surface tension of the polymer droplet, the polymer solution is charged and ejected as nanofibers are collected on the conductive target. Generally reported PAN-based carbon nanofiber diameters are around 250 nm, although there are lower diameters reached by the usage of DMSO solution [17,50]. Presented nanofibers are synthesized in the range of 230 nm (Figure 3) in the putative interval for carbon nanofibers [9]. Images of the TiO_2+PAN indicate that (Figure 3) TiO_2 nanoparticles located on the fiber edges successfully. In EDS spectra (Figure 3 D and E) obtained after electrospinning, the peaks of the Ti element were observed to be compatible with each other. Au peaks are observed because of the coating material of FESEM measurement.

3.2. Fuel cell applications

Carbon nanofibers are especially used for battery and other energy applications. Much of these secondary battery studies evaluate the capacitance performance of PAN and its composites with nanoparticles for example, as sodium–selenium batteries [51], long-life sodium-ion batteries [52], Li–S batteries [9]. FCs and batteries diversify excessively, and one of the FC types is voltage induced one [53,54] as exhibited in the presented study. To examine the different voltage inputs for the FCs 3.5 and 9 V, initial voltages were applied to the FC systems. Obtained cell parameters are presented at the consecutive sections.

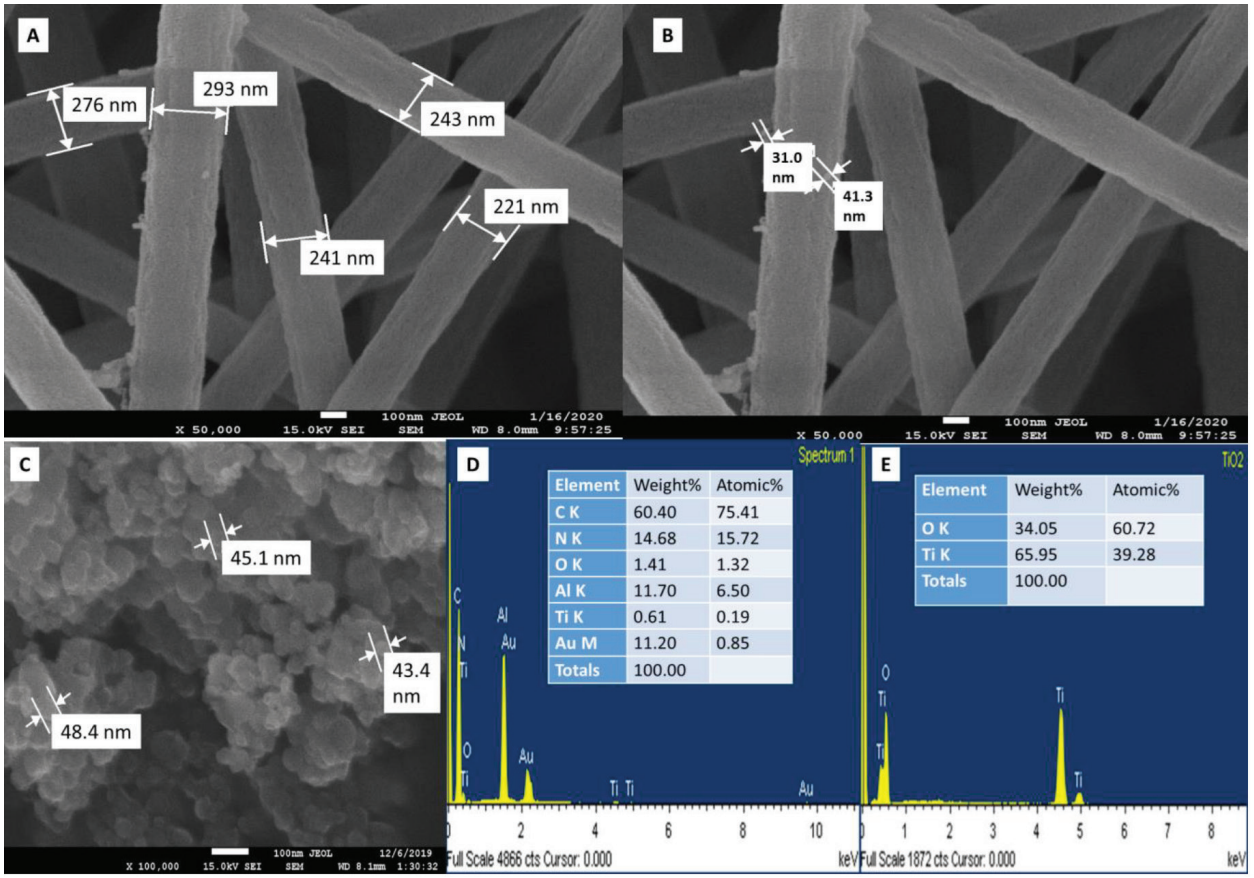

Figure 3. FESEM images of A) fiber size indicated TiO_2+PAN, B) the size of the TiO_2 indicated in TiO_2+PAN, C) synthesized TiO_2 nanoparticles before electrospinning, D) EDS spectrum of TiO_2+PAN, E) EDS spectrum of TiO_2 nanoparticles.

3.2.1. 3.5 V initial potential applied electrolysis cell measurements

DBC, PGE, TiO_2+PAN/DBC, and TiO_2+PAN/PGE electrodes were utilized as cathodes where DBC was employed as the anode in the 0.1 M 200 mL of $NaNO_{3(aq)}$ solution electrolyte filled single-cell FC, and polarisation graphics were obtained. Firstly, DBC cathode was examined and showed 29.39 mA cm^{-2} current density and 13.18 mW cm^{-2} power density values (Figure 4A). Subsequently, PGE cathode showed 31.43 mA cm^{-2} current density and 41.01 mW cm^{-2} power density (Figure 4B), whereas TiO_2+PAN/DBC showed 63.24 mA cm^{-2} current density and 17.64 mW cm^{-2} values (Figure 4C). Finally, TiO_2+PAN/PGE electrode showed 62.54 mA cm^{-2} current density and 20.94 mW cm^{-2} power density (Figure 4D).

When the results are evaluated, it is certain that TiO_2+PAN nanofiber modification enriched the current and power density values approximately three-fold for DBC and PGE. Besides the results it has been indicated that PGE based electrodes exhibited lower but quite similar current density values with DBC electrodes but slightly reached higher power density values. In comparison, the better FC performance outputs of PGE electrodes that are made of pure graphitic microbeads could be attained to the composite additives in DBC during battery production. These additives may cause an inner resistance compared to a pure graphitic electrode. Apart from these comments, the most important point of this 3.5 potential application experiments is that none of the presented FCs reached to the initial voltage value. Therefore, higher voltage application was examined for upcoming experiments.

3.2.2. 9 V initial potential applied electrolysis cell measurements

To further investigate the catalytic effect of the initial charging conditions the voltages between 3.5 and 9 V intervals were examined. Among all, 9 V was found to be applicable and consequent FCs were charged with 9 V. FC systems were measured as mentioned above at 3.5 V measurements. From the polarization graphics, DBC cathode using FC showed 0.29 A cm^{-2} current density and 0.46 W cm^{-2} power density values (Figure 5A). PGE cathode using FC showed 0.95 A cm^{-2} current density and 2.01 W cm^{-2} power density values (Figure 5B), whereas TiO_2+PAN/DBC showed 0.68 A cm^{-2} current

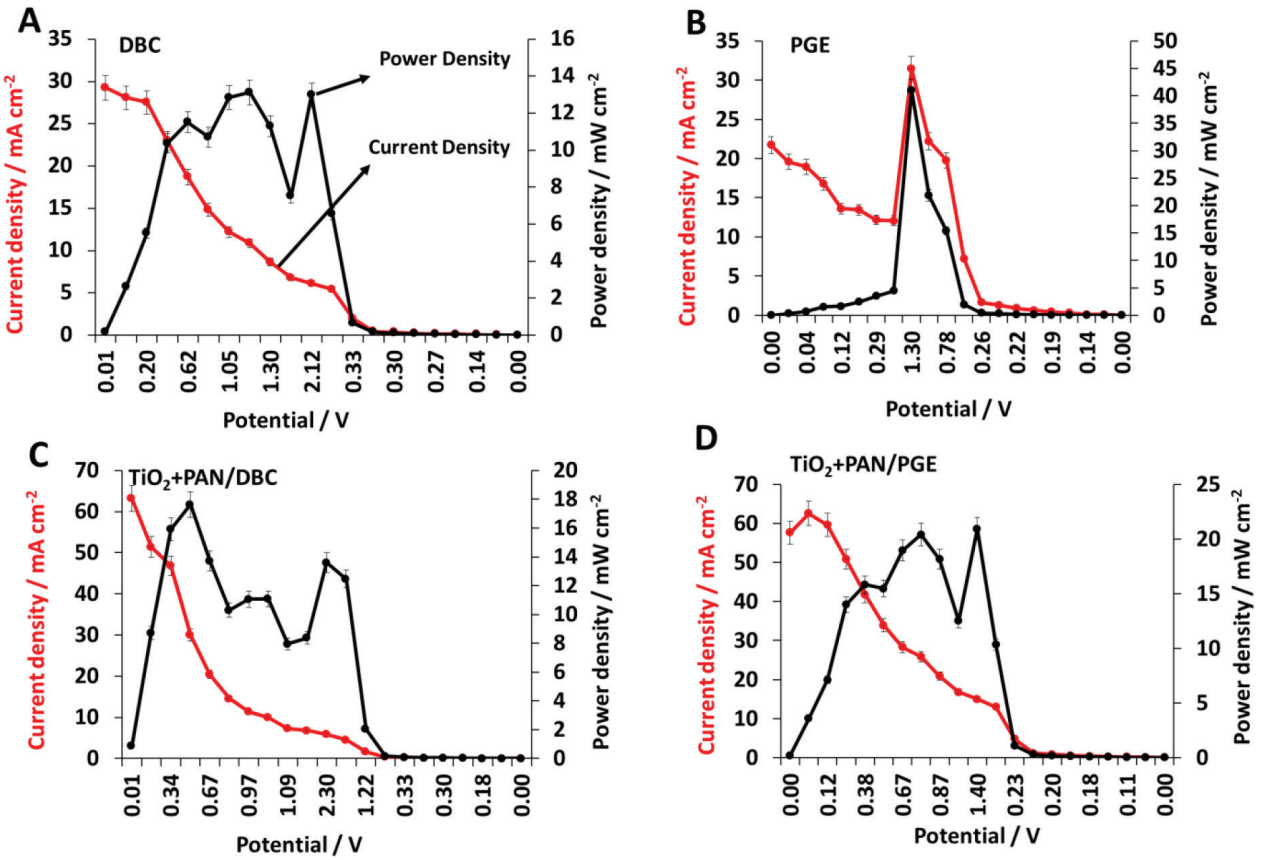

Figure 4. 3.5 V measurements of A) DBC, B) PGE, C) TiO_2+PAN/DBC, and D) TiO_2+PAN/PGE electrodes.

density and 0.62 W cm^{-2} power density values (Figure 5C). Later, TiO_2+PAN/PGE electrode showed 2.00 A cm^{-2} current density and 5.05 W cm^{-2} power density values (Figure 5E).

These results, evaluated for both 3.5 V measurements and previous works [24], show that there has been an undeniable improvement on the FC outputs due to the voltage increment. After a successful start-up, the maximum current and power densities for all electrodes were found to be a minimum fifty-fold higher than 3.5 V measurements. It is clear that 9 V provides a positive correlation for the FC system compared to 3.5 V initiated experiments for all cases. Besides, the earliest voltage began to increase strikingly when the FCs were initiated by higher voltage. It reduces the ohmic drop caused by the inner environment of the FC. Additionally, potentials obtained from the whole FC systems reached higher values that indicate the electrodes showed catalytic contribution in the FC systems. Also, the higher current and power density values were recorded at very early stages compared to the 3.5 V measurements, and observed polarization graphics were more stable in terms of voltage drops. Moreover, when the TiO_2+PAN/DBC and TiO_2+PAN/PGE electrodes were compared to their bare DBC and PGE electrodes' results, there have been reasonable increments, respectively. These results suggested that the electrospinning of electrodes with TiO_2 doped PAN greatly enhance the power generation.

3.3. Electrochemical characterization of PGE and TiO_2+PAN/PGE

After the impressive progress results on the FC performances of PGE based electrodes, electrochemical activity of untreated and electrospun PGE electrodes was investigated. The CV is generally used to explain the electrochemical mechanism of the electrode with EIS. Here, it is observed that TiO_2+PAN/PGE electrode showed a cathodic peak position of 0.17 V peak height, 0.06 mA. Anodic peak position 0.36 V; 0.05 mA, these peaks are nearly reversible (Figure 6A). This shows the electron transfer on the electrode surface is in equilibration for both reduction and oxidation. When the peak heights and peak potentials of TiO_2+PAN/PGE are taken into account cathodic peak position showed a shift to the lower potential as 0.16 V and peak height reached the 0.12 mA value besides, anodic peak position is 0.41 V and the peak height is 0.09 mA. This means that the reduction capacity of the electrode is increased by the electrospinning, it might be because of the excellent supercapacitor feature of PAN [24]. Additionally, TiO_2 nanoparticles clearly increased the peak current nearly ten folds compared to the results of the PGE electrode (Figure 6A). Of course, these results are needed to be in correlation with

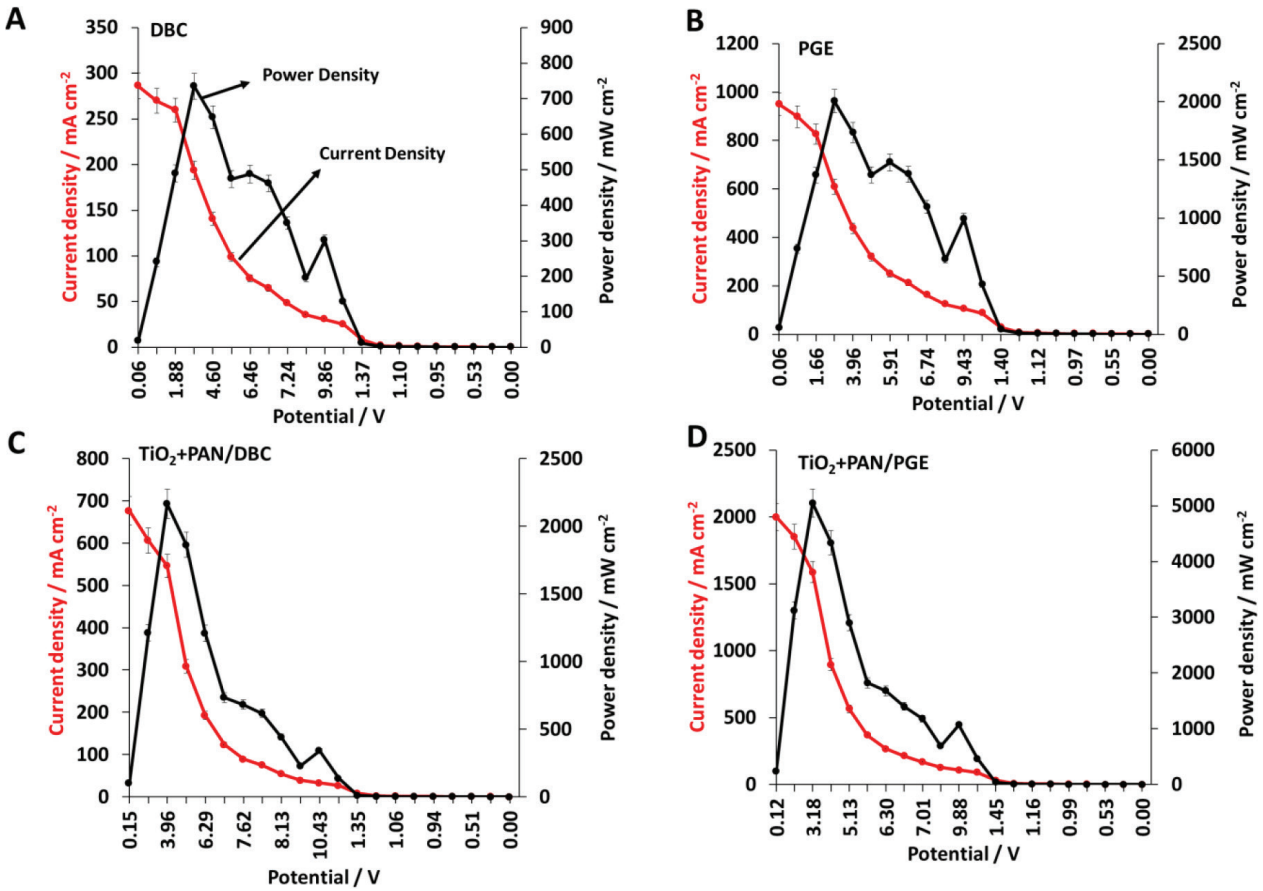

Figure 5. 9 V measurements of A) DBC, B) PGE, C) TiO_2+PAN/DBC, and D) TiO_2+PAN/PGE electrodes.

impedimetric results. EIS is a reliable technique that has been used to investigate a wide range of experimental systems with very different electrochemical properties [55]. In the given section, EIS measurements of PGE, and TiO_2+PAN/PGE electrodes are evaluated by three different types of plots named as Nyquist (Figure 6B), bode-phase (Figure 6C and Figure 6E) and Lissajous (Figure 6D and Figure 6F) plots. Nyquist plots are composed of two main parts: semicircle and linear. In an impedance mechanism, if impedance on the electrode surface increases, the semicircle part shows a larger radius but if diffusion of the electrons is higher semicircle gets smaller and linear part shows a higher slope. If the dominant effect in the electrochemical reaction mechanism is diffusion, this type of impedance is called Warburg impedance [56]. Figure 6B shows that TiO_2+PAN/PGE shows a Warburg type of an impedance spectrum while PGE exhibits two serial semicircles. These results can be evaluated more clearly on Figure 6C and Figure 6E bode plots. Figure 6C and Figure 6E are the bode plots of PGE and TiO_2+PAN/PGE electrodes, respectively. As the semicircle wanes and linear part increased, diffusion-controlled electron transfer was triggered and conductivity of the electrode increased. These semicircles are observed at PGE based electrode twice while TiO_2+PAN/PGE based electrode has one semicircle relatively with a smaller radius in accordance with the CV measurements.

The ohmic resistance behaviors of PGE and TiO_2+PAN/PGE electrodes were also evaluated. The frequency dependence of ΔV value (900 mV) and the corresponding Lissajous plots are shown in Figure 6D and Figure 6F. Figure 6D and Figure 6F are Lissajous plots of PGE and TiO_2+PAN/PGE electrodes, respectively. As shown in the figures, a sigmoidal response is obtained for a 900 mV input amplitude when the ohmic resistance is large for PGE, whereas a linear response is seen for the TiO_2+PAN/PGE when the ohmic resistance is small. This result is consistent with Nyquist and bode-phase measurement results [57]. Finally, fitting analysis was conducted to evaluate the surface behavior of the TiO_2+PAN/PGE electrode (Figure 5G). The best fitting circuit was obtained for [R(RQ)(RQ)] with the lowest estimated error as 0.2 % through fitting, and given as inset in Figure 6G [58]. Here Q denotes either capacitance or resistance in the circuit. It has been seen that hydrophobic nature of PAN nanofiber produced a capacitance or resistance on the surface. Capacitance property of the nanofiber is enhanced by the TiO_2 nps in the composite structure [47].

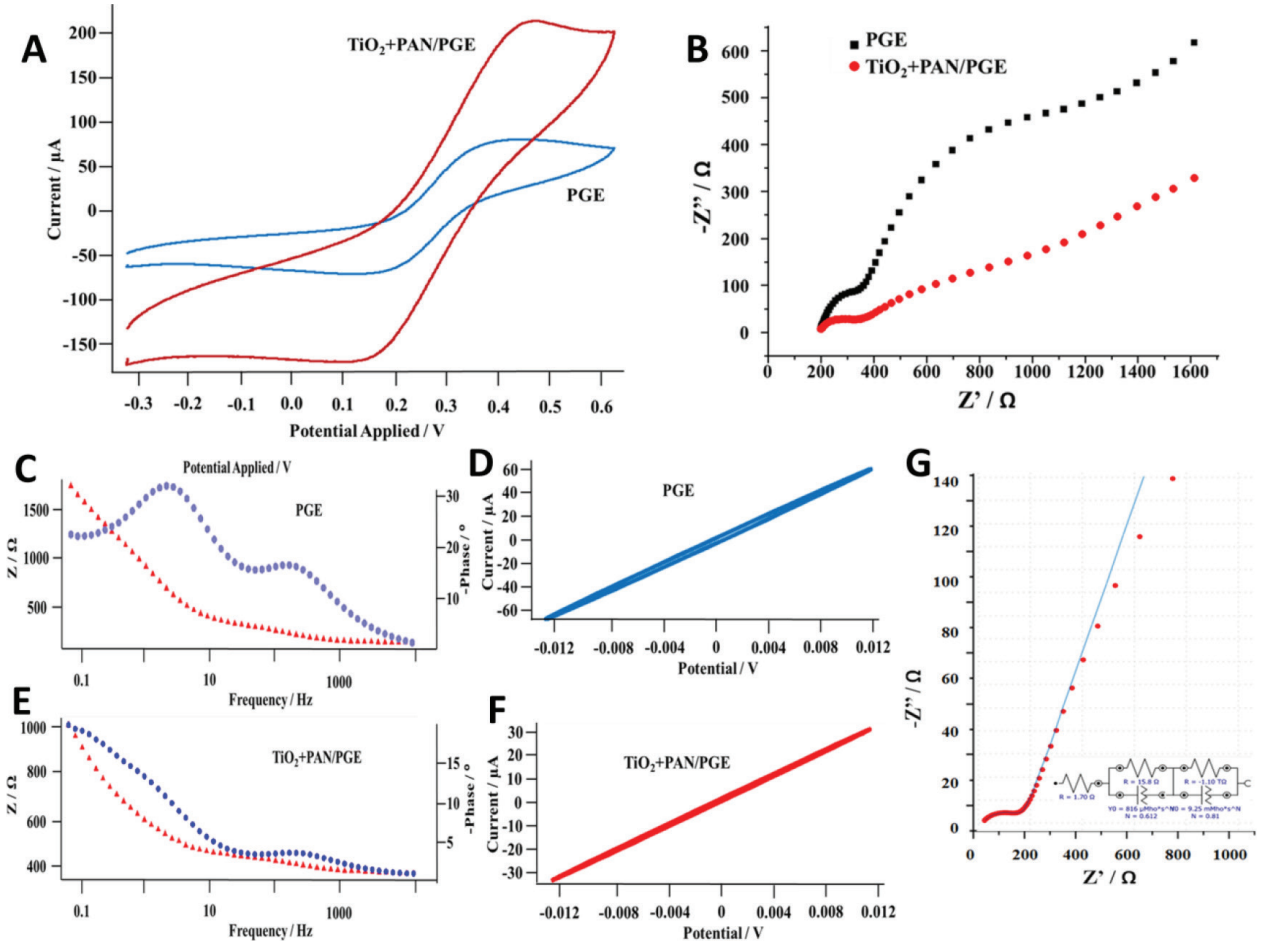

Figure 6. CV and EIS measurements of PGE and TiO_2+PAN/PGE electrodes. A) Voltammograms, B) Nyquist plot, C) and E) Bode-phase plots, D) and F) Lissajous plots, G) The circuit and the fitting analysis of TiO_2+PAN/PGE electrode's Nyquist plot.

3.4. Long-term recovery measurements

The long-term stability of the developed electrodes in FC systems was examined after one-month measurements. All of the above-mentioned electrodes were utilized to the EC systems as cathodes in the same conditions with initial measurements, with 9 V loading. Results are given with the recovery values in brackets. Consecutively DBC, PGE, TiO_2+PAN/DBC, and TiO_2+PAN/PGE electrodes were utilized as cathodes in EC systems, and polarisation graphics were obtained. DBC cathode showed 0.27 A cm^{-2} current density (96%) and 0.61 W cm^{-2} power density (67%) values (Figure 7A), PGE electrode showed 0.91 A cm^{-2} current density (96%) and 2.18 W cm^{-2} power density (91%) (Figure 7B), whereas TiO_2+PAN/DBC showed 0.68 A cm^{-2} current density (99.8%) and 0.59 W cm^{-2} power density (96%) values (Figure 7C), and TiO_2+PAN/PGE electrode showed 1.98 A cm^{-2} current density (99%) and 5.49 W cm^{-2} power density (91%) (Figure 7D). Here the results indicate that even the power and current density of the TiO_2+PAN/PGE electrode is remarked as the best values, the recoveries of these measurements are lower than other electrodes. This is attributed to the high current and voltage occurrence on this electrode at once, this creates a perturbation on the thousand grade power output values, hence they are still over 90%'s.

Rauf et al. (2018) [24] reported that generally commercial Pt/C electrocatalyst and the maximum power density could reach to 0.7–1 W cm^{-2} and Ponce de Leon et al. (2006) [59] reported a range of FC studies, in which obtained power outputs are lower of compatible to presented study. These are just a few samples and can be multiplied to give sight to the applicability of the presented FC system for both of the DBC or PGE. Evaluating the final performances of PGE or DBC based electrodes, in sight of the FC operations a standardized and fast responding and high power outputs providing electrode should be preferred meanly PGE based one. Besides, DBC is also promising in terms of power outputs, but it might be explained in detail in terms of the battery components or stable current production capabilities, which can be more useful when investigated in other electrochemical applications.

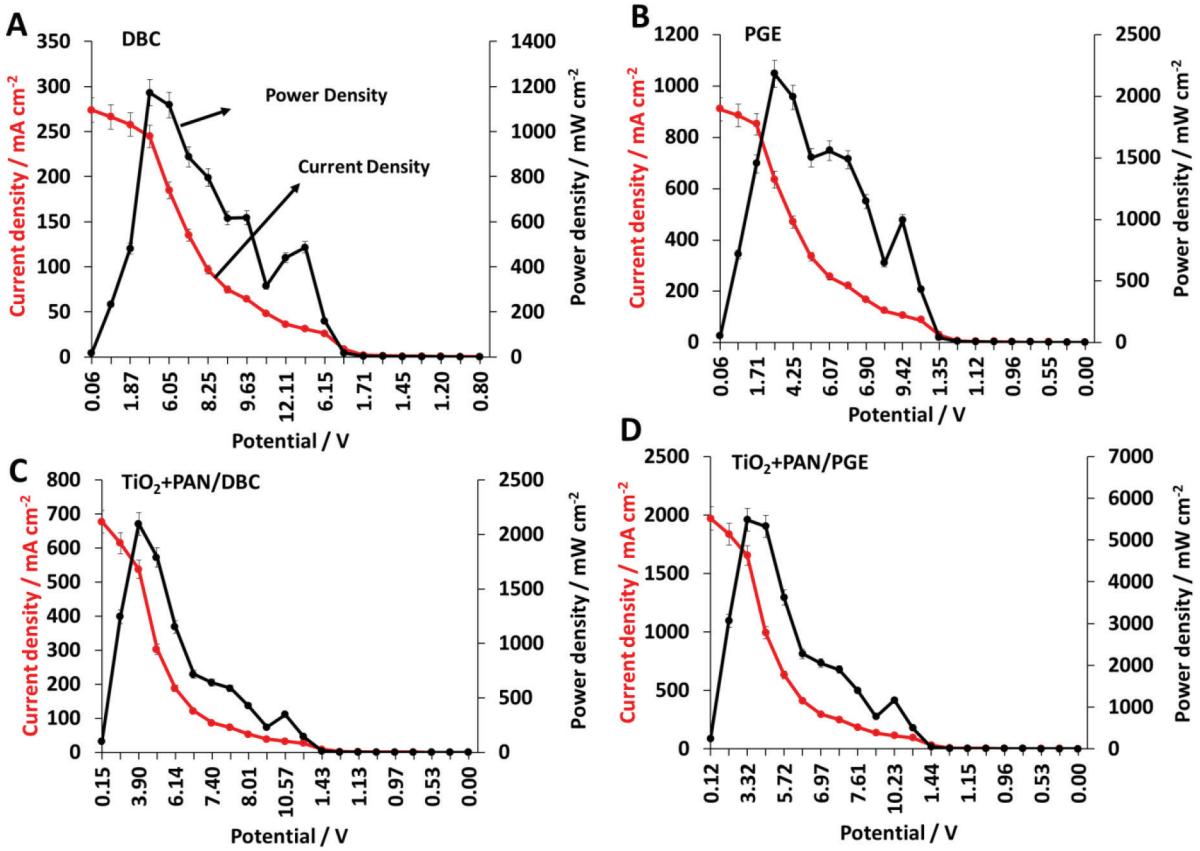

Figure 7. Long-term stability measurements of A) DBC, B) PGE, C) TiO_2+PAN/DBC, and D) TiO_2+PAN/PGE electrodes.

4. Conclusion

Overall, PGE-based electrodes showed a better ten-fold increase in electrochemical activity than DBC for FC applications. Both electrodes exhibited higher FC performance at high voltages, the best results were obtained using TiO_2+PAN/PGE as 2.00 A cm^{-2} current density and 5.05 W cm^{-2} power density values. After one month of measurements, electrode recoveries for current and power density performances were 99% and 91%, respectively. It has been found that the results can be improved by selecting a suitable conductive polymer for electrospinning. Based on the promising results in terms of this study, the recovery of discarded batteries needs to be explored and expanded with their use in future FC or biosensor studies.

Acknowledgments

The author is grateful to Prof. Dr. Hülya KARA SUBAŞAT (Muğla Sıtkı Koçman University, Institute of Graduate Studies in Science and Engineering, Head of the Energy Department) and Prof. Dr. M. Hamdi KARAOGLU (Muğla Sıtkı Koçman University, Department of Chemistry) for their contributions.

References

1. Asmatulu R, Khan WS. Electrospun nanofibers for catalyst applications. In: Synthesis and Applications of Electrospun Nanofibers. Amsterdam, The Netherlands: Elsevier, 2019, pp. 153-173. https://doi.org/10.1016/B978-0-12-813914-1.00008-0.

2. Kara H, Oylumluoglu G, Coban MB. Photoluminescence properties of a new Sm(III) Complex/PMMA electrospun composite fibers. Journal of Cluster Science 2020; 31: 701-708. https://doi.org/10.1007/s10876-019-01677-7.

3. Ligon C, Latimer K, Hood ZD, Pitigala S, Gilroy KD et al. Electrospun metal and metal alloy decorated TiO_2 nanofiber photocatalysts for hydrogen generation. RSC Advances 2018; 8: 32865-32876. https://doi.org/10.1039/C8RA04148B.

4. Cagil EM, Ozcan F, Ertul S. Fabrication of calixarene based protein scaffold by electrospin coating for tissue engineering. Journal of Nanoscience and Nanotechnology 2018; 18: 5292-5298. https://doi.org/10.1166/jnn.2018.15381.

5. Chen G, Wang Y, Fan L, Xiong X, Zhu C et al. Electrospun CuWO4 nanofibers for visible light photocatalysis. Materials Letters 2019; 251: 23-25. https://doi.org/10.1016/j.matlet.2019.05.032.

6. Oylumluoglu G, Coban MB, Kocak C, Aygun M, Kara H. 2-and 1-D coordination polymers of Dy(III) and Ho(III) with near infrared and visible luminescence by efficient charge-transfer antenna ligand. Jornal of Molecular Structure 2017; 1146: 356-364. https://doi.org/10.1016/j.molstruc.2017.06.020.

7. Coban MB, Erkarslan U, Oylumluoglu G, Aygun M, Kara H. Hydrothermal synthesis, crystal structure and photoluminescent properties; 3D Holmium(III) coordination polymer. Inorganica Chimica Acta 2016; 447: 87-91. https://doi.org/10.1016/j.ica.2016.03.038.

8. Tyagi A, Singh N, Sharma Y, Gupta RK. Improved supercapacitive performance in electrospun TiO2 nanofibers through Ta-doping for electrochemical capacitor applications. Catalysis Today 2019; 325: 33-40. https://doi.org/10.1016/j.cattod.2018.06.026.

9. Wu K, Hu Y, Shen Z, Chen R, He X et al. Highly efficient and green fabrication of a modified C nanofiber interlayer for high-performance Li–S batteries. Journal of Materials Chemistry A 2018; 6: 2693-2699. https://doi.org/10.1039/C7TA09641K.

10. Powers D, Wycisk R, Pintauro PN. Electrospun tri-layer membranes for H2/Air fuel cells. Journal of Membrane Science 2019; 573: 107-116. https://doi.org/10.1016/j.memsci.2018.11.046.

11. Kong W, Zhang M, Han Z, Zhang Q. A theoretical model for the triple phase boundary of solid oxide fuel cell electrospun electrodes. Applied Science 2019; 9: 493. https://doi.org/10.3390/app9030493.

12. Ahn M, Cho J, Lee W. One-step fabrication of composite nanofibers for solid oxide fuel cell electrodes. Journal of Power Sources 2019; 434: 226733. https://doi.org/10.1016/j.jpowsour.2019.226749.

13. Cai T, Huang M, Huang Y, Zheng W. Enhanced performance of microbial fuel cells by electrospinning carbon nanofibers hybrid carbon nanotubes composite anode. International Journal of Hydrogen Energy 2019; 44: 3088-3098. https://doi.org/10.1016/j.ijhydene.2018.11.205.

14. Oroujzadeh M, Etesami M, Mehdipour-Ataei S. Poly(ether ketone) composite membranes by electrospinning for fuel cell applications. Journal of Power Sources 2019; 434: 226733. https://doi.org/10.1016/j.jpowsour.2019.226733.

15. Zizhou RE, Çay A, Akçakoca Kumbasar EP, Çolpan CÖ. Production of poly(vinyl alcohol)/Nafion® nanofibers and their stability assessment for the use in direct methanol fuel cells. Journal of Industrial Textiles 2019; 50 (6): 1-21. https://doi.org/10.1177/1528083719844611.

16. Jian Fang TL, Wang X. Nanofibers-Production, Properties and Functional Applications. London, UK: InTech, 2011. https://doi.org/10.5772/916.

17. Kurban Z, Lovell A, Jenkins D, Bennington S, Loader I et al. Turbostratic graphite nanofibres from electrospun solutions of PAN in dimethylsulphoxide. European Polymer Journal 2010; 46: 1194-1202. https://doi.org/10.1016/j.eurpolymj.2010.03.015.

18. Padmavathi R, Sangeetha D. Synthesis and characterization of electrospun carbon nanofiber supported Pt catalyst for fuel cells. Electrochimica Acta 2013; 112: 1-13. https://doi.org/10.1016/j.electacta.2013.08.078.

19. Zussman E, Chen X, Ding W, Calabri L, Dikin DA et al. Mechanical and structural characterization of electrospun PAN-derived carbon nanofibers. Carbon 2005; 41: 2175-2185. https://doi.org/10.1016/j.carbon.2005.03.031.

20. Zhang X, Huang Y, Zhou X, Wang F, Luo Z et al. Characterizations of carbonized electrospun mats as diffusion layers for direct methanol fuel cells. Journal of Power Sources 2020; 448: 227410. https://doi.org/10.1016/j.jpowsour.2019.227410.

21. Lai C, Kolla P, Zhao Y, Fong H, Smirnova A. Lignin-derived electrospun carbon nanofiber mats with supercritically deposited Ag nanoparticles for oxygen reduction reaction in alkaline fuel cells. Electrochimica Acta 2014; 130: 431-438. https://doi.org/10.1016/j.electacta.2014.03.006.

22. Aydın H, Çelik SÜ, Bozkurt A. Electrolyte loaded hexagonal boron nitride/polyacrylonitrile nanofibers for lithium ion battery application. Solid State Ionics 2017; 309: 71-76. https://doi.org/10.1016/j.ssi.2017.07.004.

23. Yousef A, Brooks RM, El-Newehy MH, Al-Deyab SS, Kim HY. Electrospun Co-TiC nanoparticles embedded on carbon nanofibers: Active and chemically stable counter electrode for methanol fuel cells and dye-sensitized solar cells. International Journal of Hydrogen Energy 2017; 42: 10407-10415. https://doi.org/10.1016/j.ijhydene.2017.01.171.

24. Rauf M, Wang JW, Zhang P, Iqbal W, Qu J et al. Non-precious nanostructured materials by electrospinning and their applications for oxygen reduction in polymer electrolyte membrane fuel cells. Journal of Power Sources 2018; 408: 17-27. https://doi.org/10.1016/j.jpowsour.2018.10.074.

25. Stassi A, Gatto I, Baglio V, Passalacqua E, Aricò AS. Investigation of Pd-based electrocatalysts for oxygen reduction in PEMFCs operating under automotive conditions. Journal of Power Sources 2013; 222: 390-399. https://doi.org/10.1016/j.jpowsour.2012.09.002.

26. Gup R, Gökçe C, Dilek N. Seven-coordinated cobalt(II) complexes with 2,6-diacetylpyridine bis(4-hydroxybenzoylhydrazone): synthesis, characterisation, DNA binding and cleavage properties. Supramolecular Chemistry 2015, 27, 629-641. https://doi.org/10.1080/10610278.2015.1051978

27. Su C, Hong BY, Tseng CM. Sol-gel preparation and photocatalysis of titanium dioxide. Catalysis Today 2004; 96: 119-126. https://doi.org/10.1016/j.cattod.2004.06.132

28. O'Regan B, Grätzel M. A low-cost, high-efficiency solar cell based on dye-sensitized colloidal TiO2 films. Nature 1991; 353: 737-740. https://doi.org/10.1038/353737a0.

29. Ondersma JW, Hamann TW. Measurements and modeling of recombination from nanoparticle TiO 2 electrodes. Journal of American Chemical Society 2011; 133: 8264-8271. https://doi.org/10.1021/ja201333u.

30. Elakkiya S, Arthanareeswaran G, Ismail AF, Das DB, Suganya R. Polyaniline coated sulfonated TiO 2 nanoparticles for effective application in proton conductive polymer membrane fuel cell. European Polymer Journal 2019; 112: 696-703. https://doi.org/10.1016/j.eurpolymj.2018.10.036.

31. Drew K, Girishkumar G, Vinodgopal K, Kamat PV. Boosting fuel cell performance with a semiconductor photocatalyst: TiO 2/Pt-Ru hybrid catalyst for methanol oxidation. The Journal of Physical Chemistry B 2005; 24: 11851-11857. https://doi.org/10.1021/jp051073d.

32. Shim J, Lee CR, Lee HK, Lee JS, Cairns EJ. Electrochemical characteristics of Pt-WO3/C and Pt-TiO2/C electrocatalysts in a polymer electrolyte fuel cell. Journal of Power Sources 2001; 102: 172-177. https://doi.org/10.1016/S0378-7753(01)00817-5.

33. Yousef A, Brooks RM, El-Newehy MH, Al-Deyab SS, Kim HY. Electrospun Co-TiC nanoparticles embedded on carbon nanofibers: active and chemically stable counter electrode for methanol fuel cells and dye-sensitized solar cells. International Journal of Hydrogen Energy 2017; 42: 10407-10415. https://doi.org/10.1016/j.ijhydene.2017.01.171

34. Mirshekari GR, Shirvanian AP. A comparative study on catalytic activity and stability of TiO_2, TiN, and TiC supported Pt electrocatalysts for oxygen reduction reaction in proton exchange membrane fuel cells environment. Journal of Electroanalytical Chemistry 2019; 840: 391–399. https://doi.org/10.1016/j.jelechem.2019.03.077

35. Tański T, Matysiak W, Krzemiński Ł. Analysis of optical properties of TiO2 nanoparticles and PAN/TiO2 composite nanofibers. Materials and Manufacturing Processes 2017; 32 (11): 1218-1224. http://dx.doi.org/10.1080/10426914.2016.1257129

36. Qiao Y, Li CM, Bao SJ, Bao QL. Carbon nanotube/polyaniline composite as anode material for microbial fuel cells. Journal of Power Sources 2007; 170: 79-84. https://www.researchgate.net/deref/http%3A%2F%2Fdx.doi.org%2F10.1016%2Fj.jpowsour.2007.03.048

37. Qiao Y, Bao SJ, Li CM, Cui XQ, Lu ZS et al. Nanostructured polyaniline/titanium dioxide composite anode for microbial fuel cells. ACS Nano 2008; 2: 113-119. https://doi.org/10.1021/nn700102s

38. Adachi M, Shimomura T, Komatsu M, Yakuwa H, Miya A. A novel mediator–polymer-modified anode for microbial fuel cells. Chemical Communications 2008; 7: 2055-2057. https://doi.org/10.1039/B717773A

39. Chen S, He G, Carmona-Martinez AA, Agarwal S, Greiner A et al. Electrospun carbon fiber mat with layered architecture for anode in microbial fuel cells, Electrochemistry Communications 2011; 13: 1026-1029. https://www.researchgate.net/deref/http%3A%2F%2Fdx.doi.org%2F10.1016%2Fj.elecom.2011.06.009

40. Špaček J, Eksin E, Havran L, Erdem A, Fojta M. Fast enzyme-linked electrochemical sensing of DNA hybridization at pencil graphite electrodes. Application to detect gene deletion in a human cell culture. Journal of Electroanalytical Chemistry 2020; 862: 113951. https://doi.org/10.1016/j.jelechem.2020.113951.

41. Gökçe G, Ben Aissa S, Nemčeková K, Catanante G, Raouafi N et al. Aptamer-modified pencil graphite electrodes for the impedimetric determination of ochratoxin A. Food Control 2020; 115: 107271. https://doi.org/10.1016/j.foodcont.2020.107271.

42. Aslan S, Aka N, Karaoğlu MH. NaOH impregnated sepiolite based heterogeneous catalyst and its utilization for the production of biodiesel from canola oil. Energy Sources, Part A: Recovery, Utilization, and Environmental Effects 2019; 41: 290-297. https://doi.org/10.1080/15567036.2018.1516010.

43. Bal Altuntaş D, Nevruzoğlu V, Dokumacı M, Cam Ş. Synthesis and characterization of activated carbon produced from waste human hair mass using chemical activation. Carbon Letters 2019; 30: 307-313. https://doi.org/10.1007/s42823-019-00099-9.

44. Chen LC, Tien CH, Ou SL, Lee KY, Tian J et al. Perovskite CsPbBr 3 quantum dots prepared using discarded lead-acid battery recycled waste. Energies 2019; 12: 1117. https://doi.org/10.3390/en12061117.

45. Yu W, Yang J, Li M, Hu Y, Liang S et al. A facile lead acetate conversion process for synthesis of high-purity alpha-lead oxide derived from spent lead-acid batteries. Journal of Chemical Technology & Biotechnology 2019; 94: 88-97. https://doi.org/10.1002/jctb.5748.

46. Li L, Ge J, Wu F, Chen R, Chen S et al. Recovery of cobalt and lithium from spent lithium ion batteries using organic citric acid as leachant. Journal of Hazardous Materials 2010; 176: 288-293. https://doi.org/10.1016/j.jhazmat.2009.11.026.

47. Aslan S, Bal Altuntaş D, Koçak Ç, Kara Subaşat H. Electrochemical evaluation of titanium (iv) oxide/polyacrylonitrile electrospun discharged battery coals as supercapacitor electrodes. Electroanalysis 2021; 33 (1): 120-128. 10.1002/elan.202060239.

48. Aslan S. The usage of discarded battery coals as electrodes and improving their hydrogen gas production performances by impregnation with Zr and Ce metals. Eurasian Journal of Biological and Chemical Sciences 2019; 2: 97-101. http://dergipark.org.tr/en/pub/ejbcs/issue/50501/597092

49. Yin H, Wada Y., Kitamura T., Kambe S., Murasawa S et al. Hydrothermal synthesis of nanosized anatase and ruffle TiO2 using amorphous phase TiO2. Journal of Materials Chemistry 2001; 11: 1694-1703. https://doi.org/10.1039/b008974p.

50. Li M, Han G, Yang B. Fabrication of the catalytic electrodes for methanol oxidation on electrospinning-derived carbon fibrous mats. Electrochemistry Communications 2008; 10: 880-883. https://doi.org/10.1016/j.elecom.2008.04.002.

51. Wang H, Jiang Y, Manthiram A. Long cycle life, low self-discharge sodium-selenium batteries with high selenium loading and suppressed polyselenide shuttling. Advanced Energy Materials 2018; 8: 1701953. https://doi.org/10.1002/aenm.201701953.

52. Yao S, Cui J, Huang J, Huang JQ, Chong WG et al. Rational assembly of hollow microporous carbon spheres as p hosts for long-life sodium-ion batteries. Advanced Energy Materials 2018; 8: 1702267. https://doi.org/10.1002/aenm.201702267.

53. Linares R, Raël S, Berger K, Hinaje M, Lévêque J. PEM single fuel cell as a dedicated power source for high-inductive superconducting coils. International Journal of Hydrogen Energy 2018; 43: 5913–5921. https://doi.org/10.1016/j.ijhydene.2017.09.013.

54. Zihrul P, Hartung I, Kirsch S, Huebner G, Hasché F et al. Voltage cycling induced losses in electrochemically active surface area and in h 2 /air-performance of PEM fuel cells. Journal of Electrochemical Society 2016; 163: F492-F498. https://doi.org/10.1149/2.0561606jes.

55. Macdonald JR. Impedance spectroscopy. Annals of Biomedical Engineering 1992; 20: 289-305. https://doi.org/10.1007/BF02368532.

56. Preis W, Hofer J, Sitte W. Characterization of electrical properties of n-conducting barium titanate as a function of dc-bias and ac-voltage amplitude by application of impedance spectroscopy. Journal of Solid State Electrochemistry 2015; 19: 2439-2444. https://doi.org/10.1007/s10008-015-2896-6.

57. Hirschorn B, Tribollet B, Orazem ME. On selection of the perturbation amplitude required to avoid nonlinear effects in impedance measurements. Israel Journal of Chemistry 2008; 48: 133-142. https://doi.org/10.1560/ijc.48.3-4.133.

58. Choe HB, Lee HS, Ismail MA, Hussin MW. Evaluation of electrochemical impedance properties of anti- corrosion films by arc thermal metal spraying method. International Journal of Electrochemical Science 2015; 10: 9775-9789.

59. de Leon CP, Walsh FC, Pletcher D, Browning DJ, Lakeman JB. Direct borohydride fuel cells. Journal of Power Sources 2006; 155: 172-181. https://doi.org/10.1016/j.jpowsour.2006.01.011.